Materials Physics and Mechanics 37 (2018) 42-51 Received: December 22, 2017

VISCOSITY-DRIVEN ATTENUATION OF ELASTIC GUIDED WAVES IN LAYERED COMPOSITE STRUCTURES

A.A. Eremin

Institute for Mathematics, Mechanics and Informatics, Kuban State University, Stavropolskaya St., 149, Krasnodar, 350040, Russia

e-mail: eremin_a_87@mail.ru

Abstract. Along with the amplitude and dispersion directivity, conditioned by the material anisotropy, source-induced elastic guided waves in layered fiber-reinforced polymer composite structures exhibit non-neglectable attenuation due to the polymer matrix viscosity. The latter should be adequately accounted for in ultrasonic nondestructive testing and structural health monitoring systems for their reliable operation. In the current paper, the influence of attenuation on guided wave propagation in anisotropic laminates is investigated experimentally and numerically. In the computational model, viscosity driven wave amplitude decay is addressed through the complex stiffness matrix, and semi-analytical integral approach is employed for parametric analysis. Experimental measurements are performed for piezoelectrically excited guided waves with scanning laser Doppler vibrometry technique.
Keywords: elastic guided waves; laminate composites; attenuation; linear viscoelasticity.

1. Introduction

Thin-walled structures, manufactured from fiber reinforced polymer (FRP) composites materials are increasingly used in strength-critical engineering constructions and, therefore, are among the main application areas of ultrasonic Nondestructive Evaluation (NDE) and Structural Health Monitoring (SHM) approaches [1]. Employing elastic guided waves (GWs) as the structure interrogation physical phenomenon, these techniques benefit from the ability of GWs to propagate at long ranges in plate-like geometries and to interact with various structural features.

Compared to metals, stronger attenuation of propagating waves in FRP laminate composites is observed [2]. In addition to the geometrical decay, GWs undergo damping, caused by the viscos nature of the polymer matrix. It depends not only on frequency and GW mode type but on the direction of wave propagation as well. Since extensive theoretical investigations of GW phenomenon in layered composite structures is an essential step for the development of efficient and reliable ultrasonic NDE and SHM systems, material-based attenuation should be considered in the corresponding computational models. Due to the relatively small strain rates typical for GWs, the latter is commonly achieved by assuming the material being a linear viscoelastic one [3]. In the case of time-harmonic motion, it results in the complex-valued stiffness tensor in the stress-strain relation, which replaces its pure real counterpart for the lossless elastic structure [3, 4]. On the other hand, in mesh-based simulations of transient GWs the Rayleigh damping approach is widely adopted [5].

In general, the components of the complex stiffness tensor are frequency dependent. However, experimental data for measured dispersion characteristics and wave fronts of ultrasonic bulk waves suggest that some simplifications are acceptable [6, 7]. Namely, real

http://dx.doi.org/10.18720/MPM.3712018_6

part of elastic moduli is assumed constant and hysteretic or Kelvin-Voigt models are commonly employed to handle the dynamic behavior of the complex stiffness tensor. While in the former, imaginary part of each viscoelastic constant does not depend on frequency, linear growth is assumed in the latter [3]. Although being initially adopted for bulk elastic waves, these models are widely utilized for the evaluation of GW dispersion properties when viscosity is considered [8, 9]. Available experimental results [2, 10] (very limited, up to date) for attenuation frequency dependencies of fundamental GW in laminate FRP composites show almost linear behavior. Thus, even the simplest hysteretic approach seems to be an adequate approximation for the viscosity damping, at least, in the limited frequency range of fundamental GW modes, which, nevertheless, is important for NDE and SHM applications.

The characterization of complex stiffness tensor, serving as an input for the aforementioned models, is a challenging optimization problem. It might be addressed through, e.g., low-frequency dynamic vibration tests [11] or, otherwise, with high-frequency ultrasonic interferometry methods, based on transmission of bulk elastic waves [6, 7]. Alternatively, some simplifying assumptions reducing the amount of independent imaginary parts of viscoelastic moduli or even relating them directly to the initial pure elastic stiffness tensor, have been also proposed [12, 13]. The latter might be useful as a starting point for the development of material characterization techniques, based on measured GW dispersion characteristics and attenuation curves.

In the present work, viscosity attenuation of elastic guided waves in a unidirectional carbon FRP composite material is investigated within the analytically-based computational model relying on the semi-analytical integral approach for 3D elastodynamics of laminate anisotropic structures [14]. Being a frequency-domain technique, it allows studying frequency and direction dependencies of GW dispersion and attenuation properties [14, 15], and, at the same time, evaluate transient propagation of GWs, excited by any surface or internal localized load through the efficient integral equation, based on asymptotic solutions for forced GWs [14]. Viscosity behavior of the material is handled with the hysteretic approach and its modification intending to follow the experimentally obtained attenuations of fundamental GWs. The latter are quantified for piezoelectrically induced GWs with a non-contact laser Doppler vibrometry.

2. Computation model for a viscoelastic anisotropic waveguide

Time-harmonic oscillations $\mathbf{u}(\mathbf{x},\omega)e^{-i\omega t}$, $\mathbf{u}=(u_x,u_y,u_z)$, $\mathbf{x}=(x,y,z)$, ($\omega=2\pi f$, f [Hz] is a dimensional frequency) of a plate-like traction-free anisotropic laminate $D=\{(x,y,z):|x|,|y|<\infty,-H<z<0\}$ are considered (Fig. 1). Assuming the waveguide material being a linear viscoelastic one, its dynamic behavior can be modeled by allowing complex components in the corresponding stiffness matrix: $\tilde{C}(\omega)=C(\omega)-i\eta(\omega)$, where C and η are real-valued, in general, frequency-dependent 6×6 matrixes further referred as an elastic stiffness and viscosity matrices.

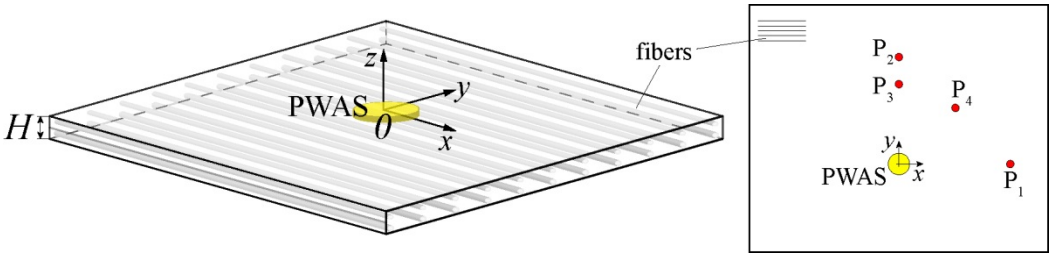

Fig. 1. Geometry of the problem: general scheme (left) and top view (right).

The structure is excited by a load $\mathbf{q}(\mathbf{x},\omega)e^{-i\omega t}$, $\mathbf{q}=(q_x,q_y,q_z)$, localized at its top surface $z = 0$ (the time-harmonic factor $e^{-i\omega t}$ is further omitted). The geometry of the considered boundary-value problem allows one to apply integral Fourier transform F_{xy} over the horizontal spatial variables x, y and to derive its explicit solution in terms of inverse Fourier two-fold path integral [14]:

$$\mathbf{u}(\mathbf{x})=\frac{1}{4\pi^2}\int\limits_{\Gamma_+}\int\limits_{0}^{2\pi}K(\alpha,\gamma,z)\mathbf{Q}(\alpha,\gamma)e^{-i\alpha r\cos(\gamma-\varphi)}d\gamma\alpha d\alpha\,, \tag{1}$$

where $K = F_{xy}[k]$ and $\mathbf{Q} = F_{xy}[\mathbf{q}]$ are Fourier symbols of the Green's matrix $k(\mathbf{x})$ and the contact stress vector $\mathbf{q}(x,y)$ (the notations of Ref. 14 and 15 are employed); coordinates (r, φ) and (α, γ) are introduced in spatial and Fourier domains, respectively. Since the poles of the matrix K elements are now complex values with positive imaginary part, the integration path Γ_+ goes in the complex plane directly along the real semi-axis Re $\alpha \geq 0$, Im $\alpha = 0$. With the residue technique and the stationary phase method, Equation (1) is reduced to the asymptotic expansion in terms of quasi-cylindrical guided waves $\mathbf{u}_n$ [14, 15]:

$$\begin{aligned}&\mathbf{u}(\mathbf{x})=\sum_{n=1}^{N_r}\mathbf{u}_n(\mathbf{x})+O((\zeta_n r)^{-1}),\ \zeta_n r\to\infty\\&\mathbf{u}_n(\mathbf{x})=\sum_{m=1}^{M_n}\mathbf{a}_{nm}(\varphi,z)e^{is_{nm}r}/\sqrt{\zeta_n r}.\end{aligned} \tag{2}$$

Here $s_{nm}=s_n(\gamma_{nm})$ are complex wavenumbers of the GWs $\mathbf{u}_n$; γ_{nm} are the stationary points of the phase functions $\hat{s}_n(\gamma)=\mathrm{Re}[\zeta_n(\gamma+\varphi+\pi/2)]\sin\gamma$: $\hat{s}_n'(\gamma_{nm})=0$; N_r is the number of poles ζ_n closest to the real axis; M_n is the number of stationary points γ_{nm} of the n-th phase function $\hat{s}_n$; amplitude factors $\mathbf{a}_{nm}$ are expressed via the residues of the product $K\mathbf{Q}$ from the poles $\zeta_n(\gamma_{nm})$. Each term in the second sum of Equations (2) is a cylindrical guided wave (CGW), specified in the radial observation direction φ by the complex wavenumber $s_{nm}(\varphi)$ and wavelength $\lambda_{nm}=2\pi/\mathrm{Re}[s_{nm}]$. The imaginary part $\chi_{nm}=\mathrm{Im}[s_{nm}(\varphi)]$ of the wave number $s_{nm}(\varphi)$ is responsible for the attenuation intensity, contributing to the Equations (2) as a decaying exponential term $\exp(-\chi_{nm}r)$. Since the lossy media is considered, energy velocities $c_{e,nm}$ should be used to characterize the speed of propagating wave packets. They are expressed in the following form [4]:

$$c_{e,nm}(\varphi)=\frac{\left\langle\mathbf{e}\cdot\mathbf{n}_\varphi\right\rangle_H}{\left\langle\mathrm{K}+\Pi\right\rangle_H}, \tag{3}$$

where the brackets $<..>_H$ denote the average over the waveguide thickness, symbol "$\cdot$" is for scalar product of complex-valued vectors, $\mathbf{e}(z)$ is the time-averaged Umov-Poynting vector, $\mathbf{n}_\varphi$ stands for the unit vector along the observation direction φ; K and Π are time-averaged kinetic and potential energy:

$$\mathrm{K}=\frac{\rho\omega^2}{4}(\mathbf{u},\mathbf{u}),\ \Pi=\frac{1}{4}\mathrm{Re}(\boldsymbol{\varepsilon},\boldsymbol{\sigma}),$$

and the six-component strain and stress vectors $\boldsymbol{\varepsilon}$ and $\boldsymbol{\sigma}$ are obtained from the corresponding tensors by means of the Voigt notation. Since Equation (3) is derived within the plane wave assumption, the displacement vector is rewritten as follows:

$$\mathbf{u}_{nm}(\mathbf{x})=\mathbf{a}_{nm}(\varphi,z)\exp[-i\varsigma_{nm}(x\cos(\gamma_{nm})+y\sin(\gamma_{nm}))],$$

and the terms $\mathbf{a}_{nm}(\varphi,z)$, ς_{nm}, γ_{nm} are taken from Equations (2).

The described computational model has been verified over the results from Ref. 8 and 9,

and it could be adopted for the simulation of time-harmonic and transient response to the forced loading of layered anisotropic waveguide as well as for the evaluation of its dispersion properties. As an example, energy velocity $c_{e,nm}$ and attenuation χ_{nm} dispersion curves of fundamental symmetric (S0), antisymmetric (A0) and shear-horizontal (SH0) modes for a unidirectional composite of thickness H = 1.12 mm and density ρ = 1482 kg/m^3 for three propagation directions (namely, $\varphi = 0$, $\varphi = \pi/4$ and $\varphi = \pi/2$) are provided in Fig. 2. This laminate represents an experimental carbon FRP sample with unidirectional $[0^o]_4$ lay-up of prepregs; fiber alignment direction coincides with the x-axis of the introduced Cartesian coordinate system (Fig. 1).

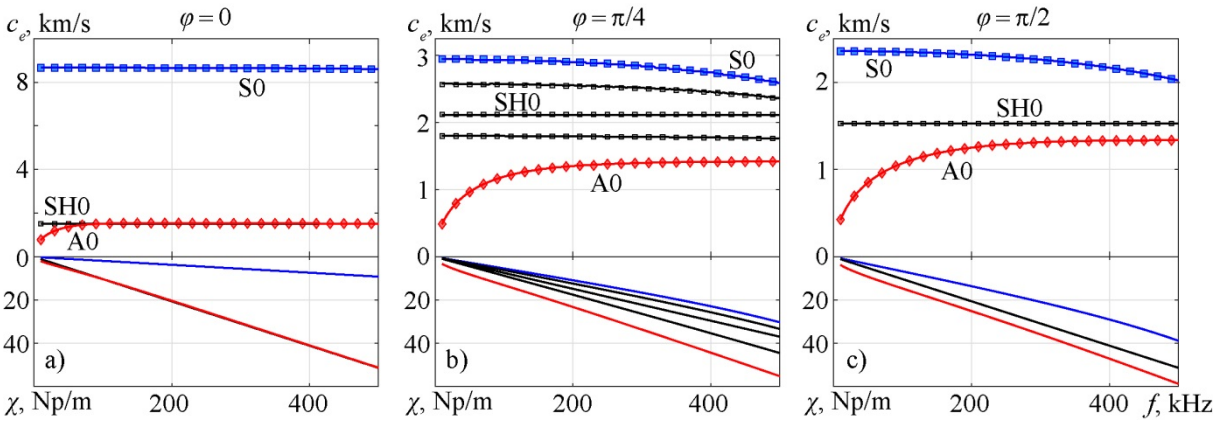

Fig. 2. Frequency dependencies of energy velocities and attenuation of fundamental modes (S0 – blue lines, SH0 – black lines and A0 – red lines) for propagation directions along the principal material axis (a, c) and for $\varphi = \pi/4$ (b); markers indicate corresponding group velocities for the pure elastic case.

Within this simulation, it is assumed that the matrices C and η do not depend on frequency (hysteretic model) and the components of the former in the principal directions of material symmetry are the following (in GPa) [16]: $C_{11} = 117.2$, $C_{22} = 10.2$, $C_{12} = 4.7$, $C_{44} = 2.55$, $C_{55} = 3.45$. Since the elements of the viscosity matrix η are initially unknown, they are chosen being proportional to the corresponding values of the elastic stiffness matrix C with the coefficient, $\theta = 0.05$, i.e., $\eta = \theta C$ [17]. Even these preliminary computations illustrate the strong influence of material anisotropy not only on energy velocities but on attenuation factors χ_{nm} as well. It is especially pronounced for χ_{S0}, which intensity in fiber direction is expectedly sufficiently smaller than in the perpendicular one (Fig. 2, a,c). On the other hand, within the current assumption about η-matrix components (further referred as Model 1), χ_{A0} varies only slightly with the propagation angle φ. The expected separation of single SH0 mode into three propagating quasi-cylindrical waves [15] is observed as well (Fig. 2, b, three black curves). Comparing to the pure elastic case (group velocities plotted with markers in Fig. 2), only minor difference is observed with the maximum relative deviation of 2%, achieved for S0 mode, propagating along the direction $\varphi = \pi/2$ at the right boundary of the frequency region considered.

3. Guided waves in a unidirectional fiber-reinforced polymer composite

Numerous experimental measurements of the transient GWs, excited with surface mounted PWAS, performed for the aforementioned unidirectional specimen [18], indicate that the attenuation of the A0 mode in the direction perpendicular to fiber alignment ($\varphi = \pi/2$) is

immensely stronger than for $\varphi = 0$. The results from Fig. 2 do not coincide with the latter, and, therefore, the values of the viscosity matrix η elements should be tuned to represent such a behavior.

Preliminarily, the frequency dependences of the attenuation factor $\chi(f)$ are measured along the material principal axis. It is related to the imaginary part of the complex wavenumber s_{nm} and might be obtained from the relation [2]:

$$\chi(f) = \frac{1}{d} \ln \left| \frac{v_z(\mathbf{x}_1, f)}{v_z(\mathbf{x}_2, f)} \cdot p \right|, \; d = |\mathbf{x}_2 - \mathbf{x}_1|, \; p = \sqrt{r_1 / r_2} \; ,$$

where $v_z(\mathbf{x}_{1,2}, f)$ is the spectrum of the out-of-plane velocities $v_z(t)$, measured at surface points $\mathbf{x}_1$ and $\mathbf{x}_2$ with the scanning laser Doppler vibrometer, d is the distance between them and p is the correction factor, which takes into account the $\sqrt{r}$ geometrical decay of quasi-cylindrical GWs according to the Equation (3). Excitation of GWs has been performed with a small circular piezoelectric wafer active sensor (PWAS) of radius $R = 3$ mm and thickness $h = 0.25$ mm. The actuator is adhesively attached to the specimen and is driven with transient voltage in the form of broadband rectangular pulse. The location of measurement points $\mathbf{x}_1$ and $\mathbf{x}_2$ is chosen in such a way that the wave packets, related to S0 and A0 modes, are well separated and, therefore, attenuation factors $\chi_{S0}(f)$ and $\chi_{A0}(f)$ might be estimated. The obtained results after averaging for, at least, four mutual locations of points $\mathbf{x}_1$ and $\mathbf{x}_2$ are summarized in Figs. 3 and 4 (green lines) for propagation directions $\varphi = 0$ and $\varphi = \pi/2$, respectively. It should be noted that there is a very high dispersion of attenuation data for S0 wave in the direction $\varphi = 0$, which is conditioned by its low out-of-plane velocity amplitudes even at high frequencies and by systematic measurements errors, occurring during the observation of an oblique-angled motion with one-dimensional scanning laser vibrometry [19]. Therefore, the confidence of the corresponding results (Fig. 3, b) is not sufficient.

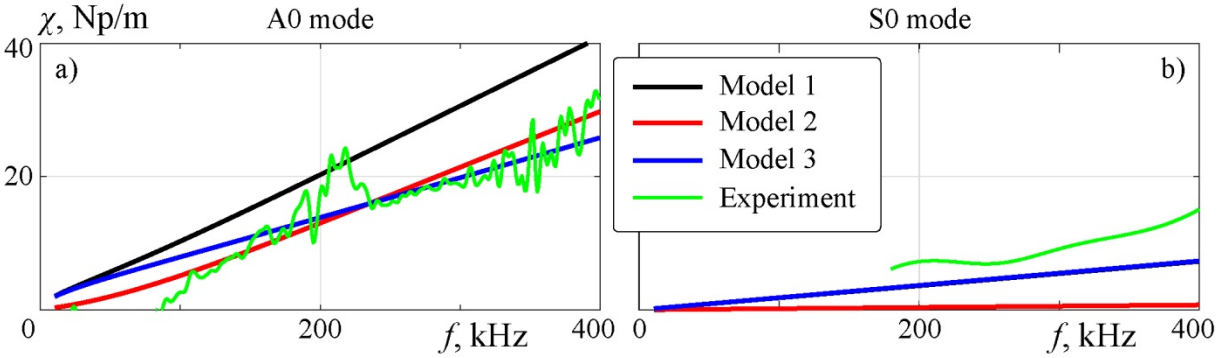

Fig. 3. Experimental (green) and computed (other colors) attenuation of fundamental A0 and S0 modes (subplots a) and b)) for propagation direction along to the fiber alignment.

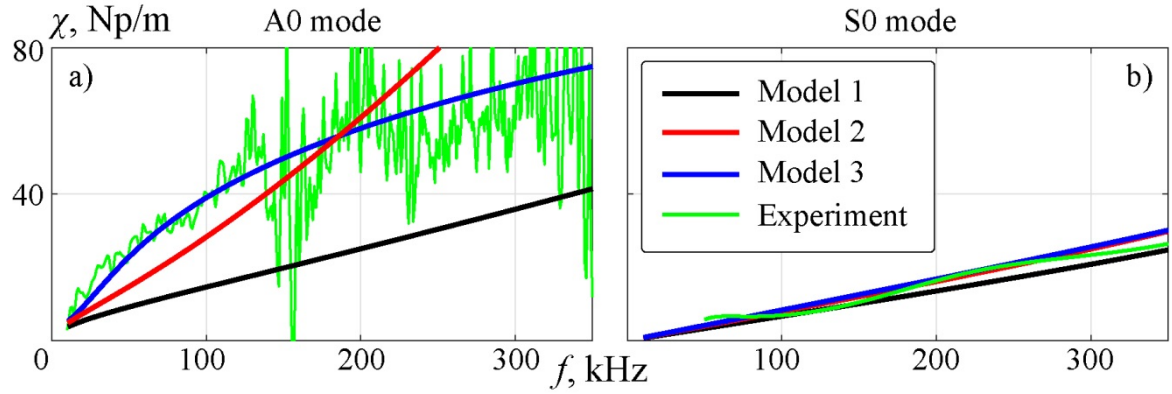

Fig. 4. Experimental (green) and computed (other colors) attenuation of fundamental A0 and S0 modes (subplots a) and b)) for propagation direction perpendicular to the fiber alignment.

The corresponding attenuation curves, obtained with the Model 1 assumption about the viscosity matrix are shown in the same figures with black lines. Though the damping of S0 mode is predicted quite adequately, the results for A0 wave do not coincide with experimental data. Since the simple variation of parameter θ does not solve this issue, a more advanced model relating $\tilde{C}, \eta$ and C matrixes has been implemented, based on the approach, proposed in Ref. [13]. In the case of a transversely isotropic elastic layer with its symmetry axis (fiber alignment direction), coinciding with the x-axis, the following relations are suggested (Model 2):

$$\tilde{C}_{ii} = C_{ii}/(1+ip\sqrt{C_{55}/C_{ii}}),\ i=1,5;\ \ \tilde{C}_{ii} = C_{ii}/(1+ip2^{i/2}\beta\sqrt{C_{55}/C_{ii}}),\ i=2,4$$
$$\tilde{C}_{12} = (C_{12}+C_{55})/(1+ip\sqrt{C_{55}/C_{ii}}) - \tilde{C}_{55},\ \tilde{C}_{23} = C_{23}/(1+ip\sqrt{C_{55}/C_{23}}). \quad (4)$$

Here parameter p is the damping factor, and β is the additional coefficient employed for the attenuation enhancement in the direction orthogonal to the symmetry axis x. Moreover, since the elements $\tilde{C}_{22}$ and $\tilde{C}_{44}$ of the complex stiffness matrix have been additionally modified, the element $\tilde{C}_{23}$ is assumed being independent from them to avoid its possible unphysical values. Considering sensitivity studies of the elastic moduli influence on GW dispersion properties [16], trial and error fitting of the computed attenuation curves to the experimental ones provides some preliminary estimations for p and β constants: $p=0.04$ and $\beta=1.75$. The corresponding χ_{A0} and χ_{S0} curves are given in Figs. 3 and 4 with red lines. Although the intensity of χ_{A0} factor for both propagation directions is represented more adequately, the slope of theoretical and experimental A0-attenuation curves does not coincide for $\varphi=\pi/2$.

Along with the stiffness matrix $\tilde{C}(\omega)$, complex compliance matrix may be formally derived: $\tilde{S}(\omega)=\tilde{C}^{-1}(\omega)$, and the corresponding set of engineering constants (Young's moduli $\tilde{E}_x$, $\tilde{E}_y$, shear moduli $\tilde{G}_{yz}$, $\tilde{G}_{xy}$ and Poisson's ratio $\tilde{\nu}_{xy}$ are all complex-valued) could be considered as the basic viscoelastic material parameters [17]. Recalling the results for pure elastic case [16], the attenuation of A0 and S0 modes in the direction $\varphi=\pi/2$ is controlled only by parameters $\tilde{E}_y$ and $\tilde{G}_{yz}$. Moreover, in the frequency range considered, the influence of $\tilde{E}_y$ on χ_{S0} is predominant. Therefore, it is suggested that the required behavior of χ_{A0} could be achieved primarily by modifying the imaginary part of $\tilde{G}_{yz}$ shear modulus and that such a modification would not produce a significant effect on χ_{S0}. According to the

curvature of the experimental χ_{A0} curve, the parameter $\tilde{G}_{yz}$ is sought in the following form:

$$\tilde{G}_{yz} = G_{xy}^{(1)} + iG_{xy}^{(2)} / \omega, \quad (5)$$

where $G_{xy}^{(1)}$, $G_{xy}^{(2)}$ are real values (Model 3). Taking the imaginary part of complex engineering constants equal to 5% of the corresponding values for the pure elastic case as an initial guess, the following complex moduli are obtained after the attenuation curve tuning (in GPa, except the Poisson's ratio): $\tilde{E}_x = 110.2 - i5.5$, $\tilde{E}_y = 8.15 - i0.5$, $\tilde{G}_{yz} = 2.55 - i0.6/\omega$, $\tilde{G}_{xy} = 3.45 - i0.1$, $\tilde{\nu}_{xy} = 0.32 - i0.01$. Simulated attenuation dispersion curves are depicted in Figs. 3 and 4 with blue lines, and the behavior of experimental A0 mode attenuation is reliably reproduced.

To illustrate the importance of accounting for the material viscosity in the simulations, experimental transient wavefields $v_z(t)$ are compared with theoretical data, computed for the described lossy models and for the ideally elastic structure. Guided waves are excited by the same small circular PWAS, which is driven with sine-windowed two-cycle sinus tone bursts with central frequencies $f_c = 120$ and 240 kHz. Due to the relatively small thickness of the actuator, the arising contact stresses $\mathbf{q}(\mathbf{x}, \omega)$ are approximated with the pin-force model [19], i.e., by ring delta-like distribution of surface radial tension [14]: $q(\mathbf{x}, \omega) = \{\tau_{rz} \cos\varphi, \tau_{rz} \sin\varphi, 0\}$, $\tau_{rz} = \delta_r(r - a)$. Wave patterns at the points $P_1(120\,\text{mm}, 0)$, $P_2(0, 120\,\text{mm})$ and $P_3(0, 80\,\text{mm})$ are shown in Figs. 5 – 7 in the normalized form. For the propagation direction along the fiber alignment (point P_1) the viscosity has only slight influence on the GW amplitudes, and the lossless model provides adequate results (Fig. 5, a). At the same time, the damping of A0 mode, predicted with Models 1 and 2, is overestimated in this frequency range ($f_c = 240\,\text{kHz}$). On the other hand, the attenuation of A0 mode in the perpendicular direction is substantial and could not be neglected, i.e., even at rather low frequencies (Fig. 6, $f_c = 120\,\text{kHz}$) the amplitude of S0 wave starts to dominate in the measured $v_z(t)$ not far away from the source. The dissipation of A0 becomes severer with the frequency growth, and even at 80 mm distant point P_3, antisymmetric wave is almost damped out at $f_c = 240$ kHz (Fig. 7). The provided computational results suggest that Models 2 and 3 are addressing A0 attenuation in an adequate way, though, as expected, with Model 2 lower frequency components of A0 are underdamped (Fig. 6, c).

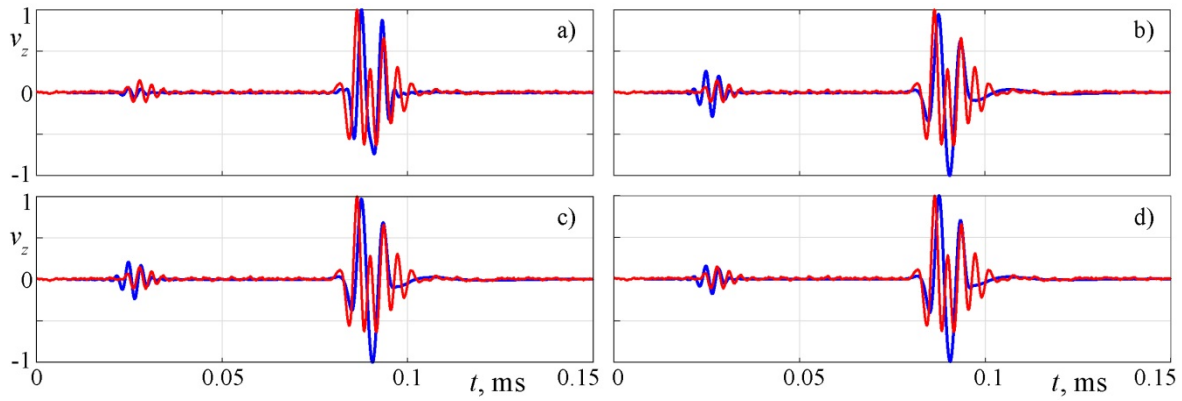

Fig. 5. Normalized measured (red line) and computed (blue line) time histories of out-of-plain velocities at surface point P_1 (ideal elastic case (a) and Models 1 – 3 (b – d)); $f_c = 240$ kHz.

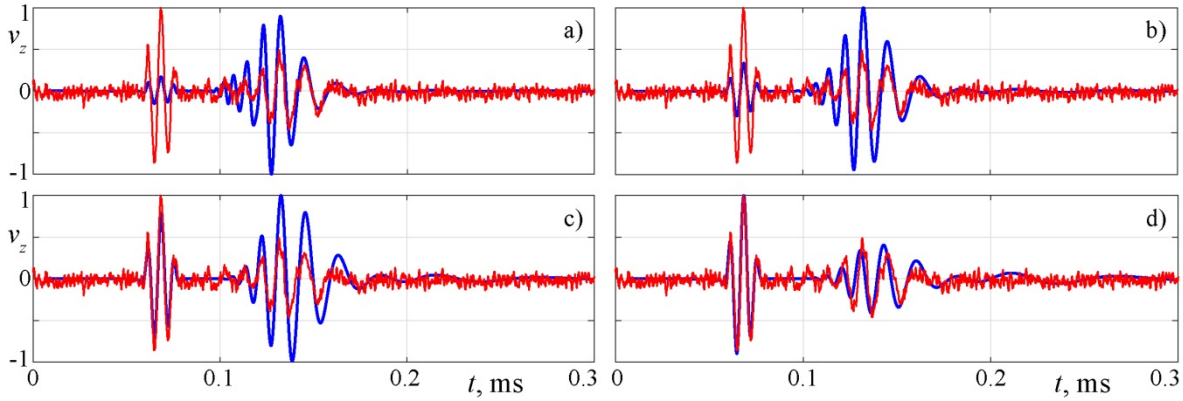

Fig. 6. Normalized measured (red line) and computed (blue line) time histories $v_z(\mathbf{x},t)$ at surface point P_2 (ideal elastic case (a) and Models 1 – 3 (b – d)); $f_c = 120$ kHz.

As an additional example, predicted and measured GW patterns for off-symmetry axis location, namely, at point $P_4(60\,\text{mm},60\,\text{mm})$ are shown in Fig. 8 for $f_c = 240$ kHz excitation. While the computations for an ideal elastic material coincide with the experimental data only in the sense of wave-packet time-of-arrival and their general form, consideration of the viscosity within Models 2 or 3 allows one to predict relative amplitudes as well. It is interesting to note that for this propagation direction $\varphi_c = \pi/4$ one of the branches of shear-horizontal wave SH0 (Fig. 2, b) is also observed both in the experiments and in the simulation. Within the three clearly distinguishable wave-packets, the latter is the middle one, arriving at the observation point after time $t = 0.05$ ms.

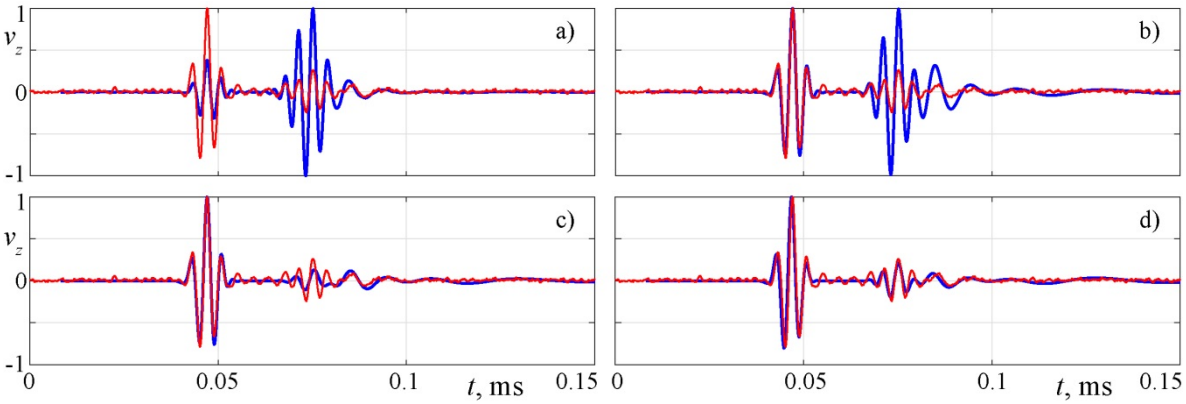

Fig. 7. Normalized measured (red line) and computed (blue line) time histories $v_z(\mathbf{x},t)$ at surface point P_3 (ideal elastic case (a) and Models 1 – 3 (b – d)); $f_c = 240$ kHz.

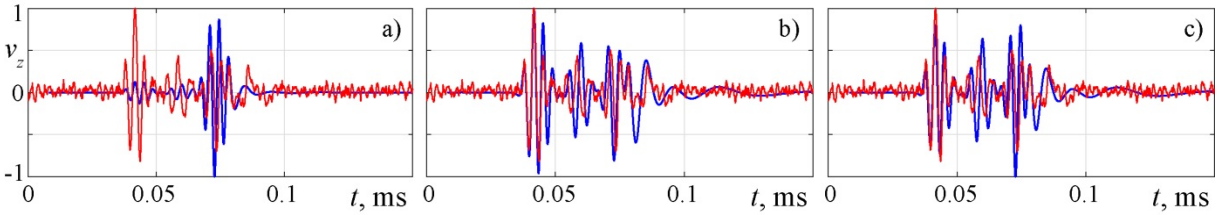

Fig. 8. Normalized measured (red line) and computed (blue line) time histories $v_z(\mathbf{x},t)$ at surface point P_4 (ideal elastic case (a) and Models 2 and 3 (b, c)); $f_c = 240$ kHz.

4. Conclusions

Analytically-based computational model for the simulation of elastic GW phenomenon in anisotropic linear viscoelastic layered waveguides has been implemented. Assuming complex-valued elastic moduli, it is capable to evaluate frequency and direction dependencies of GW dispersion properties and viscosity-conditioned attenuation. To assure the applicability of the developed model to realistic composite materials, experimental investigations for a unidirectional carbon FRP sample have been performed. Preliminarily, complex elastic constants have been estimated from experimental decay curves for fundamental GWs propagating along material symmetry axes. To handle the observed severe damping of the antisymmetric wave A0 in the direction perpendicular to fiber alignment, additional tuning of the hysteretic model has been proposed. Comparing measured and computed time histories of PWAS excited GWs, the model adequacy is confirmed.

For the future work, more sophisticated laminate lay-ups, i.e., cross-ply and quasi-isotropic ones, will be investigated and the problem of the SHM sensor network design (number and location of sensors) in the sense of additional material-conditioned GW damping will be considered.

Acknowledgements. *This work is funded by the Russian Science Foundation (Project No. 17-11-01191).*

The author expresses his deep gratitude to Prof. Evgeny Glushkov and Prof. Natalia Glushkova (Kuban State University, Krasnodar) for their encouragement and academic advices. The support of Prof. Rolf Lammering (Helmut Schmidt University, Hamburg) in laser vibrometry experiments is also highly acknowledged.

References

[1] R. Lammering, U. Gabbert, M. Sinapius, T. Schuster, P. Wierach, *Lamb-Wave Based Structural Health Monitoring in Polymer Composites* (Springer International Publishing, Cham, 2017).

[2] K. Asamene, L. Hudson, M. Sundaresan // *Ultrasonics* **59** (2015) 86.

[3] D.G. Jones, *Handbook of Viscoelastic Damping* (John Wiley & Sons, Inc., New York, 2001).

[4] B.A. Auld, *Acoustic Fields and Waves in Solids* (John Wiley & Sons, Inc., New York, 1973).

[5] M. Gresil, V. Giurgiutiu // *J. Intell. Mater. Syst. Struct.* **26** (2014) 2151.

[6] B. Hosten, M. Castaings // *J. Acoust. Soc. Am*. **94** (1993) 1488.

[7] S. Guilbaud, B. Audoin // *J. Acoust. Soc. Am.* **105** (1999) 2226.

[8] G. Neau, *Lamb Waves in Anisotropic Viscoelastic Plates. Study of the Wave Fronts and Attenuation (*PhD Thesis, L'Universite Bordeaux I, 2003).

[9] I. Bartoli, A. Marzani, F.L. di Scalea, E. Viola // *J. Sound Vib.* **295** (2006) 685.

[10] M. Calomfirescu, A.S. Herrmann // *Proc. of SPIE* **6529** (2007) 652929.

[11] H. Li, Y. Niu, C. Mu, B. Wen // *Shock and Vibration* **2017** (2017) 6395739.

[12] J.D.D. Melo, D.W. Radford // *J. Compos. Mater.* **37** (2003) 129

[13] A. Mal, S.-S. Lih // *J. Appl. Mech.* **59** (1992) 878

[14] Y.V. Glushkov, N.V. Glushkova, A.S. Krivonos // *J. Appl. Math. Mech.* **74** (2010) 297

[15] E.V. Glushkov, N.V. Glushkova, A.A. Eremin, R. Lammering // *J. Acoust. Soc. Am.* **105** (2014) 148.

[16] A.A. Eremin, E.V. Glushkov, N.V. Glushkova, R. Lammering // *Compos. Struct.* **125** (2015) 458.

[17] B. Hosten, M. Castaings // *Composites: Part A* **39** (2008) 1054.

[18] B. Hennings, R. Lammering // *Compos. Struct.* **151** (2016) 142.

[19] M.N. Neumann, B. Hennings, R. Lammering // *Strain* **49** (2013) 95.
[20] V. Giurgiutiu // *J. Intell. Material Syst. Struct.* **16** (2005) 291.